JVI Journals.ASM.org

Alphacoronavirus Protein 7 Modulates Host Innate Immune Response

Jazmina L. G. Cruz,[a]* Martina Becares,[a] Isabel Sola,[a] Juan Carlos Oliveros,[b] Luis Enjuanes,[a] Sonia Zúñiga[a]

Department of Molecular and Cell Biology, Centro Nacional de Biotecnología, CNB-CSIC, Campus Universidad Autónoma de Madrid, Madrid, Spain[a]; Computational Genomics Facility, Centro Nacional de Biotecnología, CNB-CSIC, Campus Universidad Autónoma de Madrid, Madrid, Spain[b]

Innate immune response is the first line of antiviral defense resulting, in most cases, in pathogen clearance with minimal clinical consequences. Viruses have developed diverse strategies to subvert host defense mechanisms and increase their survival. In the transmissible gastroenteritis virus (TGEV) as a model, we previously reported that accessory gene 7 counteracts the host antiviral response by associating with the catalytic subunit of protein phosphatase 1 (PP1c). In the present work, the effect of the absence of gene 7 on the host cell, during infection, was further analyzed by transcriptomic analysis. The pattern of gene expression of cells infected with a recombinant mutant TGEV, lacking gene 7 expression (rTGEV-Δ7), was compared to that of cells infected with the parental virus (rTGEV-wt). Genes involved in the immune response, the interferon response, and inflammation were upregulated during TGEV infection in the absence of gene 7. An exacerbated innate immune response during infection with rTGEV-Δ7 virus was observed both *in vitro* and *in vivo*. An increase in macrophage recruitment and activation in lung tissues infected with rTGEV-Δ7 virus was observed compared to cells infected with the parental virus. In summary, the absence of protein 7 both *in vitro* and *in vivo* led to increased proinflammatory responses and acute tissue damage after infection. In a porcine animal model, which is immunologically similar to humans, we present a novel example of how viral proteins counteract host antiviral pathways to determine the infection outcome and pathogenesis.

The order *Nidovirales* comprises enveloped single-stranded, positive-sense RNA viruses and includes the *Coronaviridae* family, which comprises viruses with the largest known RNA genome (~30 kb) (1, 2). Coronaviruses (CoVs) have been classified into three genera—*Alphacoronavirus*, *Betacoronavirus*, and *Gammacoronavirus* (3)—and a fourth, recently proposed, *Deltacoronavirus* genus (3, 4). These viruses are the causative agents of a variety of human and animal diseases. In humans, CoVs produce respiratory tract infections, ranging from the common cold to severe pneumonia and acute respiratory distress syndrome (ARDS) that may result in death (5–9). In animals, CoVs also cause life-threatening diseases, such as severe enteric and respiratory tract infections, and are economically important pathogens (10). However, there is only limited information on the molecular mechanisms governing CoV virulence and pathogenesis.

The 5′ two-thirds of the CoV genome encode the replicase proteins that are expressed from two overlapping open reading frames (ORFs) 1a and 1b (11). The 3′ third of the genome contains the genes encoding structural proteins and a set of accessory genes, whose sequence and number differ between the different species of CoV (1, 3). Generally, CoV accessory genes have been related with virulence modulation (12). Severe and acute respiratory syndrome (SARS)-CoV contains the largest number of accessory genes, and it has been proposed that these genes could be responsible for its high virulence (13, 14). A role for some structural genes, such as SARS-CoV genes E and 6, on CoV pathogenesis and virulence has also been demonstrated (14–18). Nevertheless, in general, the function of accessory genes during CoV infection requires further studies (13, 14).

Double-stranded RNA (dsRNA), produced by RNA viruses as a replication intermediate, is a pathogen-associated molecular pattern that mediates the activation of well-characterized antiviral mechanisms leading to protein synthesis shut down and the stimulation of host innate immunity for initial detection of pathogens and subsequent activation of adaptive immunity (19). The pathway that leads to a block in protein synthesis includes the activation of double-stranded RNA-dependent protein kinase (PKR), leading to eukaryotic translation initiation factor 2 (eIF2α) phosphorylation, and the activation of the 2′-5′-oligoadenylate synthetase (2′-5′OAS) and its effector enzyme, the RNase L (RNase L), responsible for RNA degradation (19, 20). The host immune response triggered by dsRNA is a key component of the innate immunity and involves activation of both proinflammatory cytokines and the type I interferon (IFN) system (21, 22).

There are three main cellular receptors for the detection of dsRNA: Toll-like receptor 3 (TLR3), retinoic acid-inducible gene I (RIG-I), and melanoma differentiation-associated gene 5 (MDA5) (22). TLR3 is located in the endosomal membrane of antigen-presenting cells, while the cytoplasmic sensors RIG-I and MDA5 are the main receptors for viral dsRNA in most cell types (20). Recently, degradation of host RNA by RNase L was proposed to be an amplifier of the innate immune response by increasing the amount of ligand involved in RIG-I and MDA5 recognition (23, 24). The signaling pathways activated by RIG-I or MDA5 recognition of dsRNA mainly lead to the activation of transcription factors IRF3/7 and NF-κB that induce the expression of type I IFN and proinflammatory cytokines (25). This innate immune response must be tightly regulated, since there is only a fine line separating the induction of a protective antiviral response and an exaggerated inflammatory response that can lead to immunopathology (26).

Due to the deleterious effects of this response on virus sur-

Received 16 April 2013 **Accepted** 24 June 2013

Published ahead of print 3 July 2013

Address correspondence to Luis Enjuanes, l.enjuanes@cnb.csic.es.

* Present address: Jazmina L. G. Cruz, Heinrich Pette Institute, Leibniz Institute for Experimental Virology, Hamburg, Germany.

doi:10.1128/JVI.01032-13

vival, many viruses have developed different strategies that counteract the host antiviral responses triggered by dsRNA (27). Many of the virus-encoded proteins with this activity identified to date interfere with multiple steps of the innate response. In addition, some viruses encode more than one gene modulating innate immunity (27). CoVs are not an exception and encode several proteins affecting type I IFN and proinflammatory cytokines production. Structural proteins, such as nucleocapsid (N) protein from several CoVs, or SARS-CoV membrane (M) protein have IFN antagonist activity (28–31). The modulation of innate immune response by CoV nonstructural protein 1 (nsp1), nsp3, and nsp16 has also been described. Nsp1 acts by promoting RNA degradation and host proteins synthesis suppression (32, 33), reducing both IFN production and signaling (34, 35). The antagonist effect of nsp3 is conserved in different CoV genera and affects IFN and proinflammatory cytokine production, although the mechanism of nsp3 action has not been determined in all cases (36–39). The IFN antagonist effect of nsp16 was recently described, involving a mechanism mediated by MDA5 recognition of non-self RNA (40). As described above, CoV accessory genes have also been related to virulence modulation. Therefore, it could be expected that some of these genes have a role in innate immunity. To date, mouse hepatitis virus (MHV) ns2, 5a, and SARS-CoV 3b and 6 proteins have been reported as IFN antagonists (28, 41, 42). Although in general the mechanisms used by accessory genes to interfere with the IFN response are not well characterized, SARS-CoV protein 6 has been studied in detail. This viral protein antagonizes both IFN production (28) and signaling by inhibiting signal transduction and activator of transcription 1 (STAT1) translocation to the nucleus (43). Further, it was recently reported that MHV ns2 protein acts as a 2′-5′-phosphodiesterase that reduces the amount of 2′-5′-oligoadenylates, avoiding the activation of RNase L and, as a consequence, reducing RNA degradation during viral infection and type I IFN production (24).

Transmissible gastroenteritis virus (TGEV) is an *Alphacoronavirus* that contains three accessory genes: 3a, 3b, and 7 (44–46). TGEV gene 7 is located at the 3′ end of the genome and is the last ORF. We have recently demonstrated that TGEV protein 7 counteracts host antiviral response and influences virus pathogenesis (47). TGEV protein 7 reduces both eIF2α phosphorylation and cellular RNA degradation by RNase L (47). The mechanism of TGEV protein 7 action is dependent on its binding to cellular protein phosphatase 1 (PP1) (47). In addition, infection with a mutant virus lacking gene 7 expression (rTGEV-Δ7) results in increased pathological damage compared to the parental (rTGEV-wt) virus (47).

In this work, to understand the molecular mechanisms leading to the increased rTGEV-Δ7 pathogenesis, the role of protein 7 on the host cell has been further analyzed by studying differential patterns of gene expression during infection with either the wild-type or mutant virus. An enhanced proinflammatory response was observed in the absence of protein 7, both *in vitro* and *in vivo*. This increased proinflammatory gene expression was associated with elevated levels of macrophage recruitment and activation in the infected tissues, being, at least in part, the cause for the enhanced tissue damage caused by viral infection in the absence of protein 7.

MATERIALS AND METHODS

Ethics statement. All animal samples used in the present study were derived from previously published *in vivo* experiments (47). As stated in the previous publication, these experiments were performed in strict accordance with EU (2010/63/UE) and Spanish (RD 1201/2005 and 32/2007) guidelines.

Virus and cells. Swine testis (ST) cells were grown in Dulbecco modified Eagle medium supplemented with 10% fetal bovine serum (48). Recombinant TGEVs, both parental (rTGEV-wt) and mutant strains lacking gene 7 expression (rTGEV-Δ7), were grown and titrated as previously described (47).

Microarray analysis. One day after achieving confluence, ST cells, grown on 35-mm-diameter plates, were mock infected or infected at an MOI of 5 with rTGEV-wt or rTGEV-Δ7. To decrease sample variability, nine independent infections were performed in each case. Samples of culture supernatants were collected for virus titration as previously described (47). Total RNA was extracted, at 6 and 12 hpi, using an RNeasy minikit (Qiagen) according to the manufacturer's instructions. RNAs were pooled three by three, obtaining three biological replicates for each experimental condition, and RNA integrity was measured in a bioanalyzer (Agilent Technologies). RNAs were biotin labeled using a One Cycle Target labeling kit (Affymetrix). Briefly, cDNA was synthesized from 5 μg of total RNA using an oligo(dT) primer with a T7 RNA polymerase promoter site added to the 5′ end. After a second strand synthesis, *in vitro* transcription was performed using T7 RNA polymerase to produce biotin-labeled cRNA. cRNA preparations (15 μg) were fragmented at 94°C for 35 min into sections of 35 to 200 bases in length and added to a hybridization solution (100 mM 4-morpholinopropanosulfonate acid, 1 M Na^+, 20 mM EDTA, 0.01% Tween 20). The cRNAs (10 μg) were hybridized to Genechip Porcine Genome Arrays (Affymetrix) at 45°C for 16 h. The arrays were stained with streptavidin-phycoerythrin and read at 1.56 μm in a GeneChip Scanner 3000 7G System (Affymetrix). Independent microarrays were hybridized for each sample.

Microarray data analysis. A robust multi-array analysis (RMA) algorithm was used for background correction, normalization, and presentation of the expression levels (49). Analysis of differential expression was performed using a Bayes moderated *t* test (limma) (50). *P* values were corrected for multiple testing using the Benjamini-Hochberg method (false discovery rate [FDR]) (51). The bioconductor packages "affy" and "limma" (www.bioconductor.org) were used for these calculations. Due to the poor Affymetrix porcine genome array annotation, an alternative one based on porcine and human gene homology was used (52). Genes were considered differentially expressed when FDR < 0.05. In addition, only genes with a fold change of >2 or of <-2 were considered for further analysis.

Functional analysis of microarray results. To understand the biological significance underlying the gene expression data, further analysis was performed. DAVID (53, 54) was used for the analysis of enriched Gene Ontology (55) "biological process" terms in the groups of up- or down-regulated genes.

RNA analysis by quantitative reverse transcription-PCR (RT-qPCR). One day after confluence, ST cells, grown on 35-mm-diameter plates, were infected at a multiplicity of infection (MOI) of 5. The total intracellular RNA was extracted at different hours postinfection (hpi) using the RNeasy minikit (Qiagen), according to the manufacturer's instructions. Viral genomic RNA (gRNA) was evaluated by RT-qPCR analysis, using a custom TaqMan assay and following standard procedures set up in our laboratory (56). Cellular gene expression was analyzed using TaqMan gene expression assays (Applied Biosystems) specific for porcine genes (Table 1). The β-glucuronidase (GUSB) gene was selected as a reference (housekeeping) gene since its expression remains constant in infected cells (independently of the rTGEV used) compared to noninfected cells. Therefore, the expression levels of each gene were corrected by the amount of housekeeping gene in each condition. The data were acquired with an ABI Prism 7000 sequence detection system and analyzed with ABI

TABLE 1 TaqMan assays

Gene[a]	Assay ID[b]	Description
CCL2 (MCP1)	Ss03394377_m1	C-C motif chemokine 2
CCL4 (MIP1B)	Ss03381395_u1	C-C motif chemokine 4
CCL5 (RANTES)	Ss03648940_m1	C-C motif chemokine 5
CXCL9	Ss03390033_m1	C-X-C motif chemokine 9
CXCL11	Ss03648935_g1	C-X-C motif chemokine 11
DDX58 (RIG-I)	Ss03381552_u1	DEAD box protein 58
GUSB	Ss03387751_u1	β-Glucuronidase
IFNB1	Ss03378485_u1	Interferon beta
IL-15	Ss03394854_m1	Interleukin 15
IRF1	Ss03388785_m1	Interferon regulatory factor 1
JAK2	Ss03394066_m1	Janus kinase 2
STAT1	Ss03392296_m1	Signal transducer and activator of transcription 1
STAT5A	Ss03394621_m1	Signal transducer and activator of transcription 5A
TGFB1	Ss03382325_u1	Transforming growth factor β1
TNF	Ss03391318_g1	Tumor necrosis factor
TNFRSF5 (CD40)	Ss03394339_m1	TNF receptor superfamily member 5
VCAM1	Ss03390912_m1	Vascular cell adhesion protein 1

[a] Alternative gene names are indicated in parentheses.
[b] TaqMan assays were used to measure porcine cellular gene expression by RT-qPCR. ID, identifier. The "Ss" in these terms refers to *Sus scrofa*.

Prism 7000 SDS version 1.2.3 software (Applied Biosystems). All experiments and data analysis were MIQE compliant (57).

PBMC isolation and cytokine analysis. Lung, blood, and serum samples were obtained from infected animals (47). Two- to three-day-old non-colostrum-deprived piglets, born from TGEV seronegative sows, were inoculated with respiratory tropism recombinant viruses (10^7 PFU/pig) according to standard procedures (58). Briefly, animals were infected by two different routes (oral and intranasal) in combination. Infected animals were monitored daily to detect symptoms of disease and death. At 0.5, 1, 2, 3, 4, and 5 days postinfection (dpi) two animals per group were sacrificed, and the samples were collected. Porcine peripheral blood mononuclear cells (PBMCs) were isolated from 8 ml of fresh heparinized venous blood by density gradient centrifugation through a Histopaque-1077 (Sigma-Aldrich) gradient according to the manufacturer's recommendations and kept frozen until their use. For their restimulation *in vitro*, PBMCs were cultured (10^6 cells/well) in 24-well plates using RPMI medium supplemented with 20% heat-inactivated fetal calf serum (FCS), 2 mM glutamine, 100 μM nonessential amino acids, and 100 U of penicillin-streptomycin/ml. After 18 h, purified TGEV (10 μg/ml) was added for stimulation, and 24 h after stimulation, total RNA was extracted. RNA extraction and RT-qPCR measurement of cellular genes was performed as described above.

Cytokine expression analysis from lung samples. At different times postinfection, lung sections from infected animals (47) were collected and stabilized with RNAlater stabilization reagent (Life Technologies) according to the manufacturer's instructions. Total RNA was extracted by using an RNeasy minikit (Qiagen) according to the manufacturer's instructions. RT-qPCR measurement of viral gRNA and cellular mRNAs was performed as described above.

Enzyme-linked immunosorbent assay (ELISA). ST cells were infected at an MOI of 5, and the culture medium was harvested at 16 hpi. Porcine tumor necrosis factor (TNF), CCL2 and IFN-β protein levels were estimated using Swine TNF ELISA kit (Invitrogen), Swine CCL2 VetSet ELISA development kit (Kingfisher Biotech), and a Pig IFNB ELISA kit (Cusabio) according to the manufacturer's instructions. The data were collected from three independent infections. In addition, CCL2 and TNF were also measured in serum samples according to the manufacturer's recommendations.

Immunofluorescence of fixed tissues. Representative sections of lung tissue were fixed with 4% paraformaldehyde and stored in 70% ethanol at 4°C (47). Paraffin embedding and sectioning were performed by the histology service in the National Center of Biotechnology (CNB-CSIC; Spain). Sections (4 μm) were deparaffined at 60°C and rehydrated by successive incubations in 100% xylol, 100% ethanol, and 96% ethanol. To unmask the antigens, tissue sections were boiled in citrate buffer (8.2 mM sodium citrate; 1.8 mM citric acid; pH 6.5) for 5 min for macrophage detection. Antigen unmasking for granulocyte detection was performed by sample incubation with 0.05% trypsin-EDTA for 30 min at 37°C. In all cases, after antigen unmasking, the samples were permeabilized with 0.25% Triton X-100 in phosphate-buffered saline (PBS) for 15 min and then blocked with 10% bovine serum albumin (BSA) and 0.25% Triton X-100 in PBS for 30 min. The samples were incubated with a monoclonal antibody that, in porcine lung samples, is specific for macrophages (4E9 [kindly provided by J. Dominguez], 1:100) (59), a monoclonal antibody that, in porcine samples (60), is specific for granulocytes (Mac387 [Dako], undiluted), or a rabbit polyclonal antibody specific for TGEV (1:100). Bound primary antibodies were detected with Alexa Fluor 488-conjugated antibody specific for mouse (Invitrogen, 1:250) or Alexa Fluor 594-conjugated antibody specific for rabbit (Invitrogen, 1:250), respectively. Cell nuclei were stained with DAPI (4′,6′-diamidino-2-phenylindole [Sigma], 1:200). Tissues were mounted in Prolong Gold antifade reagent (Invitrogen) and analyzed with a confocal fluorescence microscope (TCS SP5; Leica). Quantitative analysis of samples was performed with MetaMorph software. Positive pixels for leukocytes were calculated relative to positive pixels for TGEV infection.

Statistic analysis. Two-tailed, unpaired Student *t* tests were used to analyze difference in mean values between groups. All results were expressed as means ± the standard deviations of the means. *P* values of <0.05 were considered significant.

RESULTS

Effect of protein 7 absence on host gene expression. To analyze the impact of TGEV protein 7 on host gene expression during infection, the transcriptomes of rTGEV-wt- and rTGEV-Δ7-infected cells were compared, using porcine microarrays, at two points postinfection. It is worth noting that under the experimental conditions used here (see Materials and Methods), both for the rTGEV-wt and rTGEV-Δ7 viruses, 99% of the cells were infected, and no differences in virus titers were observed, as expected (47). MIAME-compliant results of the microarrays have been deposited in the Gene Expression Omnibus database (GEO [National Center for Biotechnology Information], accession code GSE41756). To select genes expressed at significantly different levels in cells infected with either the wild-type or mutant viruses, the threshold was established at a fold change of >2 or <-2 and a false discovery rate (FDR) of <0.05 (Fig. 1A). A comparison of infected to noninfected cells, at late times postinfection, showed more than 1,500 and 2,500 genes whose expression varied significantly between rTGEV-wt and rTGEV-Δ7 infection (Table 2). In contrast, the number of differentially expressed genes was significantly reduced when the transcriptomes of cells infected with TGEV-wt and TGEV-Δ7 were compared (Table 2). In relation to rTGEV-wt-infected cells, 26 and 301 genes were upregulated, and 84 and 466 genes were downregulated at 6 and 12 h postinfection (hpi), respectively, in rTGEV-Δ7-infected cells. More than 60% of the differentially expressed genes at 6 hpi also changed their expression at 12 hpi. These results indicated that differential gene activation during rTGEV-Δ7 infection, compared to that induced by rTGEV-wt, was maintained at 12 hpi, although additional differentially expressed genes were noted at later times postinfection.

Genes differentially expressed during TGEV infection (both up- and downregulated), in the presence or absence of protein 7,

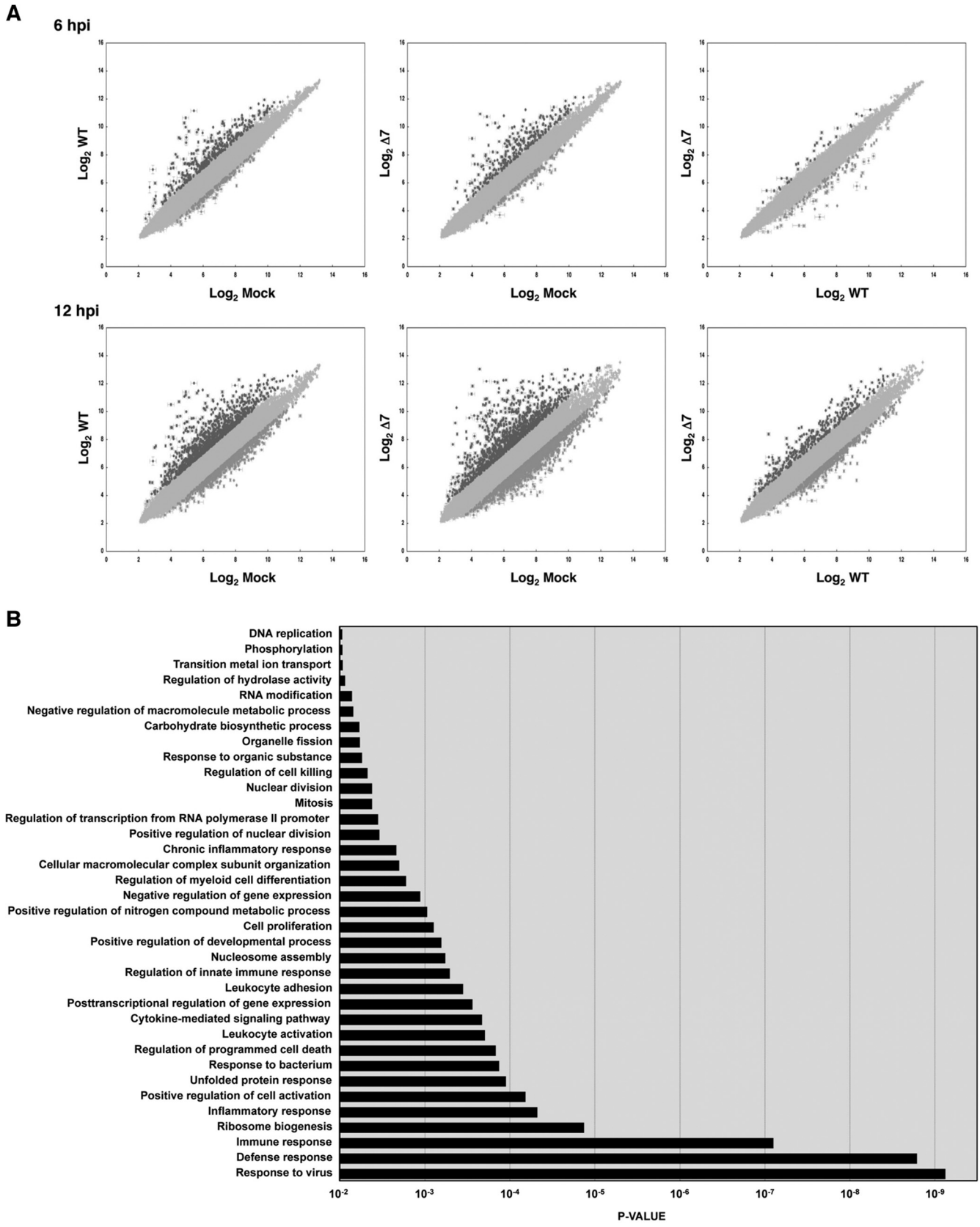

FIG 1 Effect of TGEV protein 7 on host gene expression. (A) Comparison of gene expression in ST cells at 6 and 12 hpi using microarrays. The data visualization and threshold set up for results filtering were performed with FIESTA viewer (J. C. Oliveros, 2007, http://bioinfogp.cnb.csic.es/tools/FIESTA/index.php). The graphs represent the normalized ratios for rTGEV-wt-infected versus mock-infected cells, rTGEV-Δ7-infected versus mock-infected cells, and rTGEV-Δ7-infected versus rTGEV-wt-infected cells. Dark gray spots indicate upregulated probes (fold change, >2), while medium gray spots indicate downregulated ones (fold change, <−2). Only genes with an FDR of <0.05 were considered as candidate genes. (B) Candidate genes that were differentially expressed in rTGEV-Δ7-infected cells compared to rTGEV-wt-infected ones, at 12 hpi, were grouped with reference to their GO biological process terms. Numbers on the *x* axis indicate DAVID FDR values.

TABLE 2 Analysis of host gene expression using porcine microarrays

Comparison	Time point (hpi)	No. of probes[a]	
		Upregulated	Downregulated
WT vs Mock	6	373	148
	12	1,119	768
Δ7 vs Mock	6	289	127
	12	1,259	1,782
Δ7 vs WT	6	31 (26)	98 (84)
	12	346 (301)	525 (466)

[a] Numbers in parentheses represent the numbers of different genes, since one gene could be present in the array with more than one probe. Upregulated, fold change > 2, FDR < 0.05; downregulated, fold change < −2, FDR < 0.05.

were grouped, using DAVID software (53, 54), according to the biological processes in which they could be potentially involved. Most of the genes were associated with responses against viruses, host defense response, and immune response (Fig. 1B) and there was significant overlap among the genes of these three groups. The genes included in response to virus gene ontology (GO) group mainly affected the immune response, the IFN response, and inflammation, and most of them were significantly upregulated during rTGEV-Δ7 infection compared to that by rTGEV-wt (Fig. 2A). Interestingly, analysis of the expression patterns during rTGEV-wt and rTGEV-Δ7 infections showed that, in general, genes activated during rTGEV-wt infection were also activated during rTGEV-Δ7 infection, although earlier or to a higher level than in rTGEV-wt in-

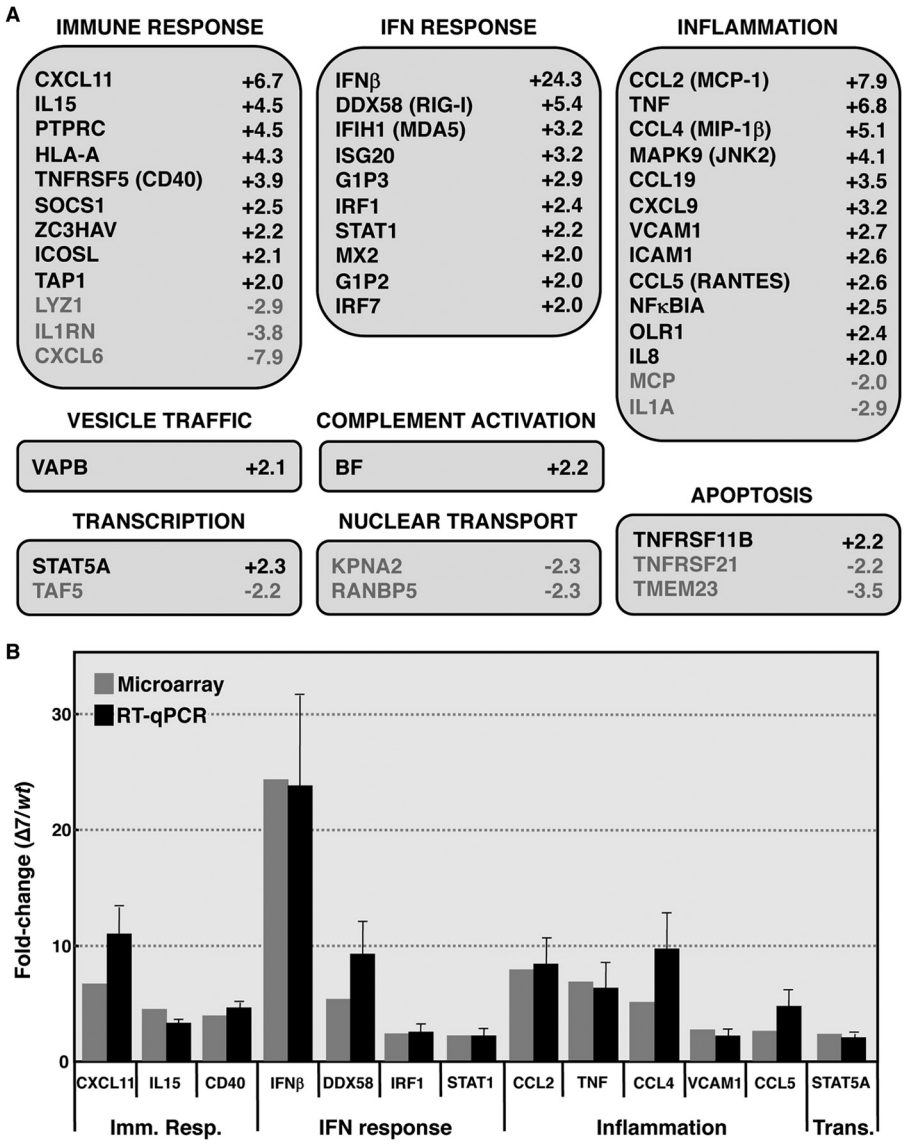

FIG 2 Host genes differentially expressed in rTGEV-Δ7 versus rTGEV-wt-infected cells. (A) Candidate genes included in response to virus GO group were classified according to their main biological functions. Black and gray lettering is used to indicate up- and downregulated genes, respectively. The numbers indicate the fold change for each gene. For genes recognized with more than one probe, the value corresponding to the greatest up- or downregulation is represented. (B) Thirteen candidate gene mRNAs were evaluated by RT-qPCR using specific TaqMan assays. RNA was extracted from rTGEV-wt- or rTGEV-Δ7-infected cells at 12 hpi. Gray bars represent the fold change obtained from microarray data. Black bars represent the data obtained by RT-qPCR. GUSB mRNA levels were used as an endogenous control in all cases. Error bars indicate the standard deviations from three independent experiments. Imm. Resp., immune response; Trans., transcription.

TABLE 3 Candidate genes selected for further study[a]

Immune category	Cytokine	Function	Fold change
Innate immunity	IFN-β	Antiviral, increased MHC class I expression	+24.3
Th1 response	IL-15	Stimulates growth and proliferation of T and NK cells	+4.5
	TNF	Local inflammation, endothelial activation; stimulates cell proliferation and induces cell differentiation	+6.8
	CXCL9	Chemotactic for activated T cells; affects the growth, movement, or activation state of cells participating in immune and inflammatory responses	+3.2
	CXCL11	Chemotactic for interleukin-activated T cells; role in diseases involving T-cell recruitment	+6.7
Chemokine	CCL2	Attracts monocytes and basophils; related to diseases characterized by monocytic infiltrates	+7.9
	CCL4	Inflammatory and chemokinetic properties	+5.1
	CCL5	Attracts monocytes, memory T-helper cells, and eosinophils; causes the release of histamine from basophils and activates eosinophils	+2.6
Others	VCAM1	Important in cell-cell recognition; influences leukocyte-endothelial cell adhesion	+2.7
Negative controls	TGFB1	Controls proliferation, differentiation, and other functions in many cell types	–1.15
	JAK2	Mediates essential signaling events in both innate and adaptive immunity	+1.67

[a] The selection was based on their differential expression levels and porcine TaqMan assay availability.

fection (data not shown). Several genes from each group were selected for RT-qPCR analysis, taking into account the availability of TaqMan assays for porcine genes detection. In all cases, RT-qPCR results confirmed the microarray results, validating the effects observed in the microarray analysis (Fig. 2B). Altogether, these data suggested that host innate immune response triggered by TGEV infection was magnified in the absence of protein 7.

Effect of protein 7 absence on innate immunity gene expression. We have previously shown that, due to protein 7 absence, rTGEV-Δ7 infection promoted an intensified host dsRNA-induced antiviral response (47). Taking this observation into account, a set of nine differentially expressed candidate genes involved in innate immunity (Table 3) was selected to study their expression kinetics by RT-qPCR. To discard a general transcription upregulation during rTGEV-Δ7 infection, which could affect the expression of all cellular genes, the mRNA levels of two other genes involved in immune response, such as JAK2 and transforming growth factor β (TGF-β), were also evaluated as controls. No differences in virus titers (data not shown) or viral gRNA accumulation (Fig. 3) were observed between the parental and mutant viruses, as expected (47). All of the selected candidate genes increased their expression during TGEV infection (Fig. 3). Interestingly, all of them were significantly upregulated in cells infected with rTGEV-Δ7, in comparison to cells infected with rTGEV-wt (Fig. 3). In contrast, control genes JAK2 and TGF-β were not differentially expressed in the absence or presence of TGEV protein 7 (Fig. 3), indicating that the increased expression of candidate genes during rTGEV-Δ7 infection was not the consequence of a general induction of host transcription.

To confirm that the elevated mRNA levels correlated with an increased protein accumulation, and attending to the availability of assays for the specific detection of porcine proteins, the levels of three cytokines (TNF, CCL2, and IFN-β) were measured during TGEV infection. TNF, CCL2, and IFN-β levels were quantified in the medium of infected ST cells using commercial ELISAs. Cells infected with rTGEV-Δ7 virus secreted higher levels (Fig. 4) of TNF (upper panels), CCL2 (medium panels) and IFN-β (lower panels) compared to rTGEV-wt-infected cells. Altogether, the data confirmed the correlation between mRNA and protein expression levels of innate immunity genes induced by rTGEV infection.

***In vivo* expression of proinflammatory cytokines in the absence of TGEV protein 7.** It was previously shown that lung damage in rTGEV-Δ7-infected pigs was greater than that observed in rTGEV-wt-infected animals (47). The observed lesions could be correlated with acute inflammation in the infected tissue (26). As described above, the data obtained in tissue culture indicate that rTGEV-Δ7 infection led to an increased expression of innate immunity-related genes, in particular of proinflammatory cytokines. To analyze whether this was also the case *in vivo*, cytokine expression in PBMCs from infected animals was studied by RT-qPCR. After *in vitro* restimulation of PBMCs from rTGEV-wt- and rTGEV-Δ7-infected animals with purified TGEV, an increase in the expression of several proinflammatory cytokines, such as TNF, CCL2, CCL5, and CXCL11, was observed (Fig. 5). TGEV infection of PBMCs was not observed, in contrast to what has been previously described, indicating that TGEV could infect pDCs (61–63). This cell type represents ca. 0.5% of the cells in a PBMC preparation (64), and pDC enrichment methods are required for the significant detection of TNF and type I IFN production by this cell type (62). Therefore, the observed increase in proinflammatory cytokines production was most likely due to re-exposure to TGEV. The levels of cytokine mRNAs were higher in PBMCs from rTGEV-Δ7-infected animals than in those from rTGEV-wt-infected animals (Fig. 5), in agreement with the results obtained in tissue culture. These data strongly suggested that rTGEV-Δ7 virus also induced a higher expression of proinflammatory cytokines *in vivo*.

To further analyze the proinflammatory cytokine levels in the infected animals, mRNA levels in lung samples were measured by RT-qPCR. Since the infection extent in the different lung sections was different, viral gRNA was also quantified, and cytokine mRNA levels were related to viral gRNA levels (Fig. 6). At 1 dpi, the mRNA levels of TNF, CCL2, and CCL5 were higher in rTGEV-Δ7-infected lungs than in rTGEV-wt-infected lungs (Fig. 6). In the case of CCL2, this increase was also found at 2 dpi (Fig. 6, middle panel). Moreover, CCL2 and TNF protein levels were measured in the sera from infected animals. Sera from rTGEV-Δ7-infected animals contained higher levels of these cytokines than those from rTGEV-wt-infected animals, particularly at early dpi (Fig. 7). Altogether, the data indicated that rTGEV-Δ7 virus also induced an exacerbated proinflammatory response *in vivo*.

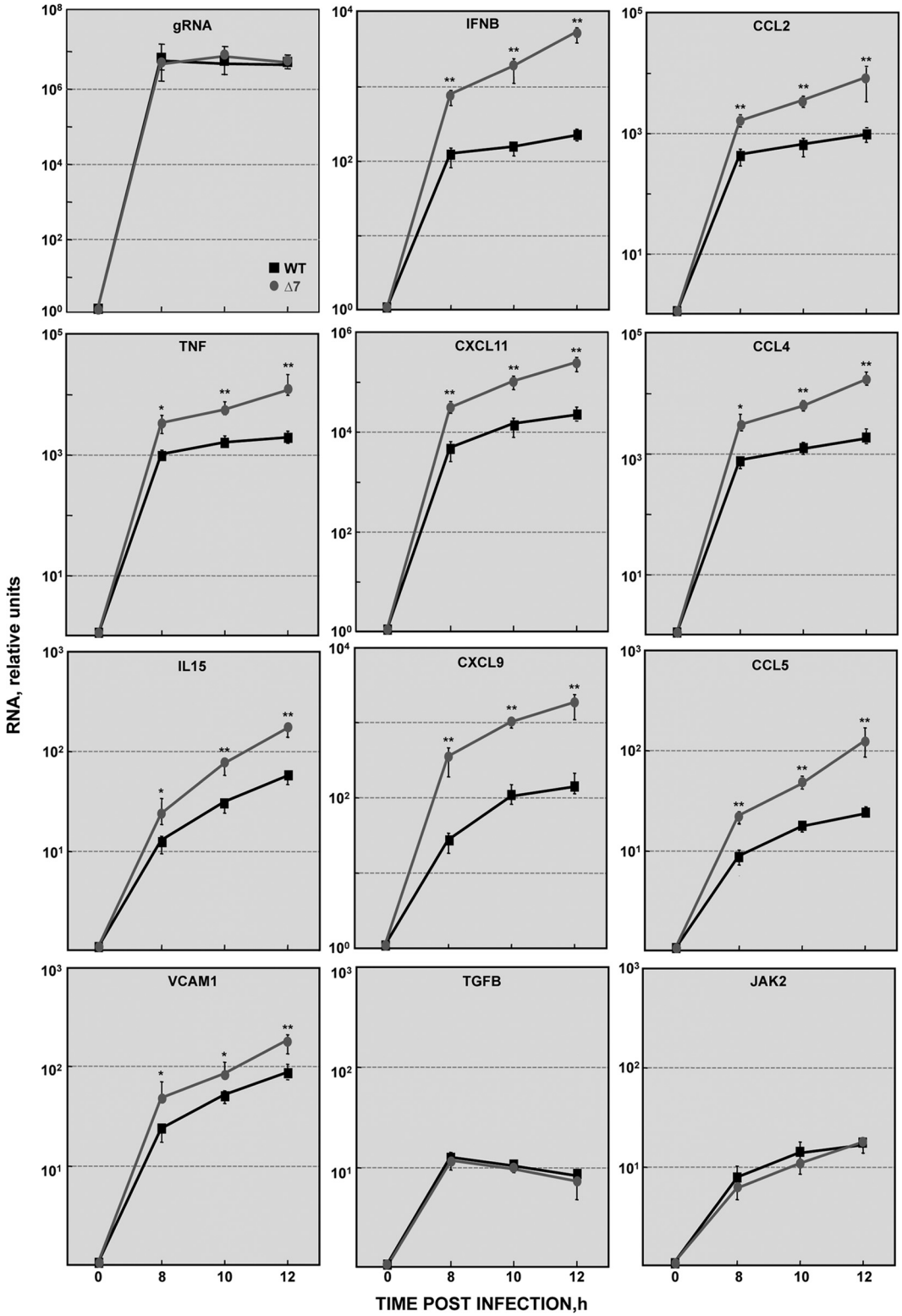

FIG 3 Expression kinetics of host genes involved in inflammation. Nine candidate genes involved in inflammation and innate immunity were selected for analysis of their expression kinetics by RT-qPCR. ST cells were infected with rTGEV-wt or rTGEV-Δ7, and the total RNA was extracted at the indicated time points. As a control for rTGEV replication, the viral gRNA levels were also evaluated. TGF-β and JAK2 were selected as negative control genes that did not change their expression levels in rTGEV-Δ7-infected cells compared to rTGEV-wt-infected cells. GUSB mRNA levels were used as an endogenous control in all cases. Error bars indicate the standard deviations from three independent experiments. **, $P < 0.01$; *, $P < 0.05$.

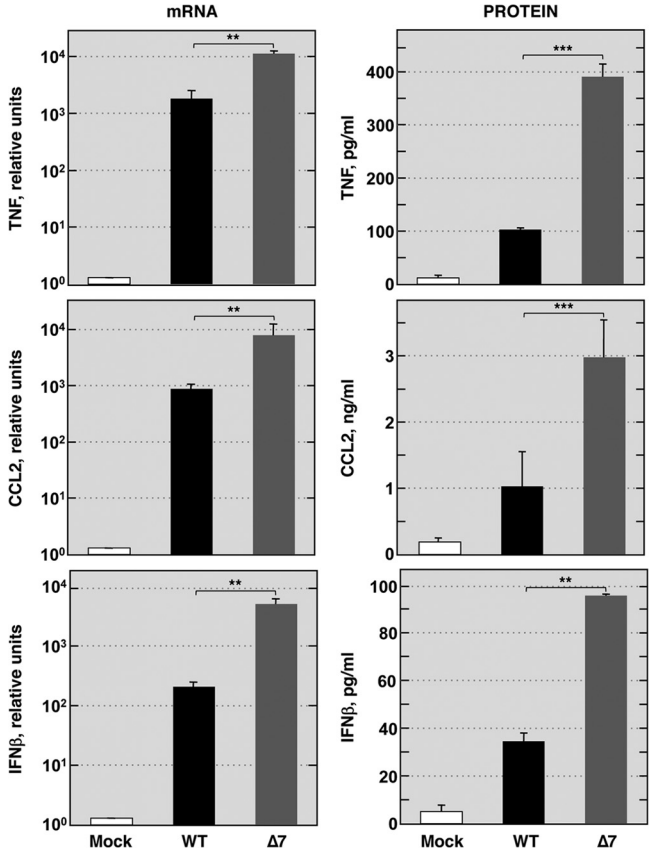

FIG 4 Host protein and mRNA levels in rTGEV-Δ7 infection. Quantification of porcine TNF (upper panels), CCL2 (middle panels), and IFN-β (lower panels) accumulation in mock-infected cells (white) or during rTGEV-wt (black) or rTGEV-Δ7 (gray) infections. At 16 hpi, mRNA accumulation was measured by RT-qPCR (left), and protein accumulation was measured by ELISA (right). Error bars indicate the standard deviations from three independent experiments. ***, $P < 0.001$; **, $P < 0.01$.

The expression of proinflammatory cytokines during infection could lead to an enhancement of tissue damage due to the activation and recruitment of leukocytes, particularly macrophages and, in some infections, neutrophils (65). These activated cells may amplify the damage produced by the pathogen, since they secrete proinflammatory cytokines potentially involved in host-mediated immunopathology (65, 66). To test this possibility, the presence of granulocytes and macrophages in the lungs of rTGEV-wt- and rTGEV-Δ7-infected animals at 1 and 4 dpi was evaluated by immunofluorescence. At 1 dpi, an increase in granulocytes was observed in both rTGEV-wt- and rTGEV-Δ7-infected tissues (Fig. 8A) that correlated with the damage observed by histopathology (47). The number of granulocytes seemed to decrease at 4 dpi in both infections (Fig. 8A), although the lung damage in rTGEV-Δ7 infection was increased compared to the one observed at 1 dpi (47). These data suggested that granulocytes were rapidly recruited at the sites of infection, as expected. The contribution of macrophages to tissue damage was analyzed by using the antibody 4E9/11 that specifically labeled porcine lysosomal associated membrane protein 1 (LAMP-1, CD107a), which mainly detects cells in an active phagocytosis state (59, 67). Therefore, this antibody allowed the simultaneous detection of both activated resident macrophages and circulating monocytes recruited into the

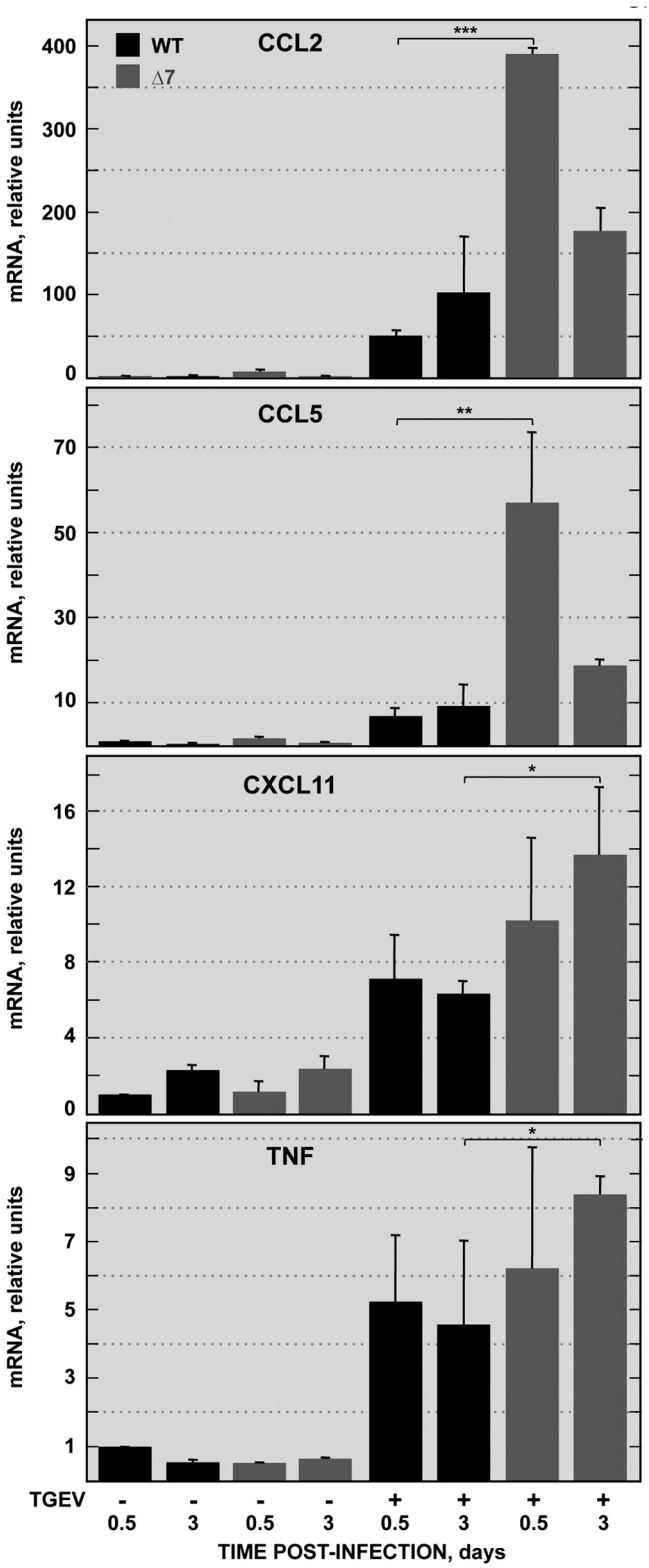

FIG 5 Expression of cytokines by PBMCs from infected animals. PBMCs from rTGEV-wt (black)- or rTGEV-Δ7 (gray)-infected animals, extracted at 0.5 and 3 dpi, were cultured and stimulated with TGEV. At 24 h after stimulation, total RNA was extracted, and the cytokine mRNA levels were analyzed by RT-qPCR. GUSB mRNA levels were used as endogenous control in all cases. Error bars indicate the standard deviations from two different animals. ***, $P < 0.001$; **, $P < 0.01$; *, $P < 0.05$.

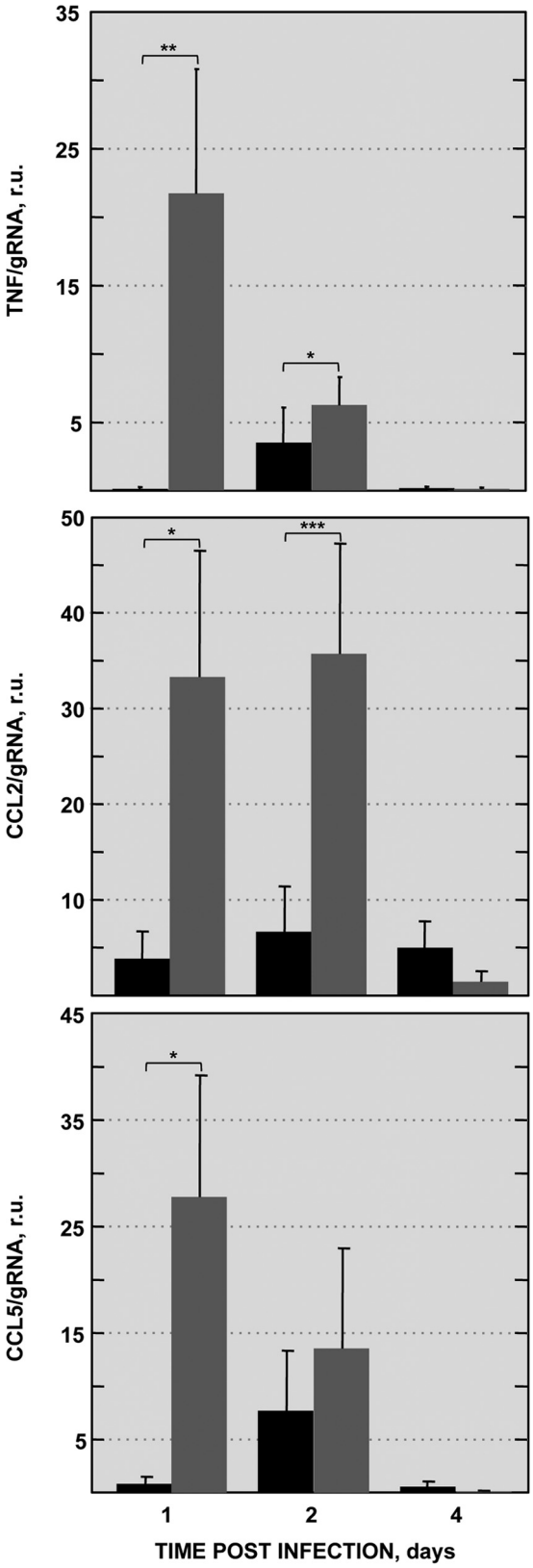

FIG 6 Expression of cytokines in lungs from infected animals. Lung fragments from rTGEV-wt (black)- or rTGEV-Δ7 (gray)-infected animals were collected at 1, 2, and 4 dpi. Total RNA was extracted, and the viral gRNA accumulation and cytokine mRNA levels were analyzed by RT-qPCR. TNF (upper panel), CCL2 (middle panel), and CCL5(lower panel) mRNA levels were determined relative to the viral gRNA in all cases. In addition, the GUSB mRNA levels were used as an endogenous control in all cases. Error bars indicate the standard deviations from two different animals. ***, $P < 0.001$; **, $P < 0.01$; *, $P < 0.05$. r.u., relative units.

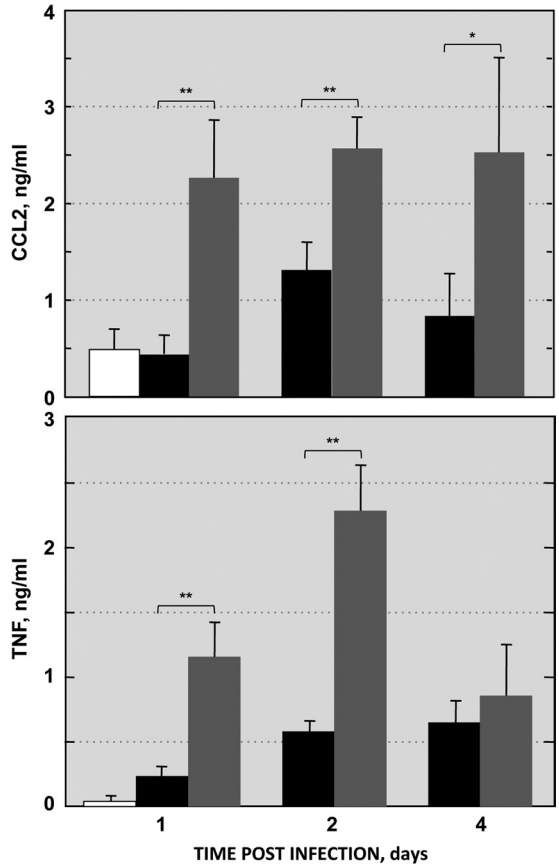

FIG 7 Cytokine levels in sera from infected animals. Quantification of porcine CCL2 (upper panel) and TNF (lower panel) accumulation in sera from mock-infected piglets (white) or animals infected with rTGEV-wt (black) or rTGEV-Δ7 (gray). Cytokine accumulation was measured by ELISA at the indicated times postinfection. Error bars indicate the standard deviations from three independent experiments. **, $P < 0.01$; *, $P < 0.05$.

site of infection, providing that they were subsequently activated. Other porcine macrophage markers, such as CD163, CD68 and CD172a, were tested. Unfortunately, the antibodies specific for these markers did not work in paraffin-embedded lung sections. An increased number of activated macrophages was observed in rTGEV-Δ7-infected lungs at 4 dpi compared to those infected with rTGEV-wt (Fig. 8B). Although it was previously reported that TGEV can replicate in alveolar macrophages (61), double-labeled cells (4E9/11$^+$ TGEV$^+$) were not detected in the lung sections at any time point analyzed. It was previously observed that rTGEV-Δ7 titers in lung were higher than those of the rTGEV-wt virus at early times postinfection (47). Therefore, the contribution of differences in tissue infection levels to leukocyte recruitment and activation was a realistic possibility. To clarify this issue, granulocyte and macrophage recruitment and activation, during rTGEV-wt and rTGEV-Δ7 infections, were estimated relative to

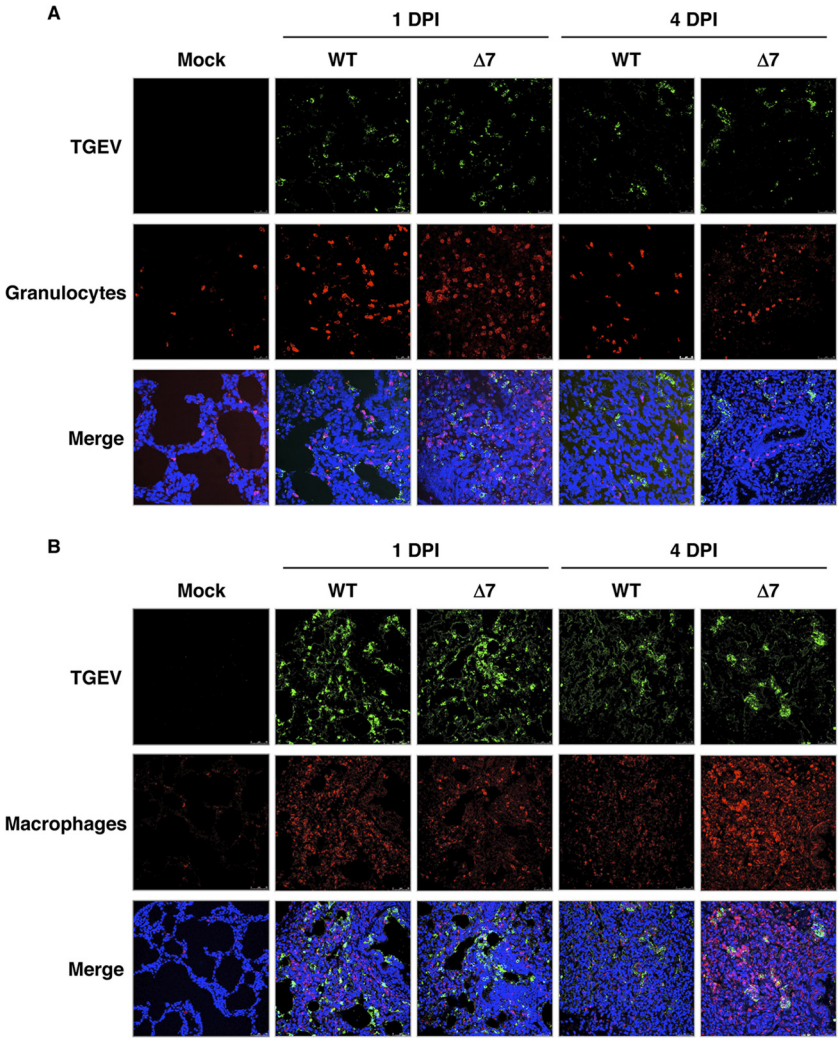

FIG 8 Leukocyte detection in lung sections from infected animals. Lung sections from noninfected (Mock) and rTGEV-wt (WT)- or rTGEV-Δ7 (Δ7)-infected piglets, at 1 and 4 dpi, were labeled with a monoclonal antibody specific for granulocytes (A) or macrophages (B) (red) and a polyclonal antibody specific for TGEV (green). Cell nuclei were labeled with DAPI (blue). Pictures were obtained by using confocal microscopy with a ×40 objective lens.

tissue infection levels in each case. Granulocyte recruitment was similar in both wild-type and mutant virus-infected tissues (Fig. 9). In contrast, at 4 dpi rTGEV-Δ7-infected tissues showed a significant increase in macrophage recruitment and activation compared to rTGEV-wt-infected tissues (Fig. 9). Altogether, these data suggested that the enhancement of lung damage produced by rTGEV-Δ7 infection was, at least in part, due to the preferential recruitment and activation of macrophages, most likely due to the increased levels of proinflammatory cytokines such as TNF or CCL2.

DISCUSSION

We have previously shown that an rTGEV lacking protein 7 expression was more virulent and caused increased pathology than the parental virus (47). To analyze the potential mechanism underlying this enhanced pathology, the patterns of gene expression after infection by each of these viruses were analyzed using microarrays covering the complete porcine genome. A marked upregulation of proinflammatory cytokine mRNA expression was observed in infections with the virus deficient in protein 7. The identification of elevated TNF, CCL2, and IFN-β confirmed the increased proinflammatory pattern at the protein level. Furthermore, similar results were obtained in *in vivo* infections, indicating that the presence of protein 7 reduced inflammatory changes after TGEV infection both in cell cultures and *in vivo*.

Viruses are good tools for understanding the molecular mechanisms modulating inflammation, especially signaling pathways that increase disease severity. The increased inflammation observed after rTGEV-Δ7 infection, caused by an exacerbated innate immune response and leading to an enhanced pathogenesis, was also described for human viruses infecting the respiratory tract, such as respiratory syncytial virus (RSV) or influenza virus. TGEV is a virus with enteric and respiratory tropism. Lung and gut infection by virulent TGEV caused significant inflammation in both tissues, and animal death is mainly due to the severe unbalance of Na^+ and K^+ ions caused by the clinical manifestation of the infection (68). It is important to note that the work described here was performed with the cell culture-adapted TGEV used in the

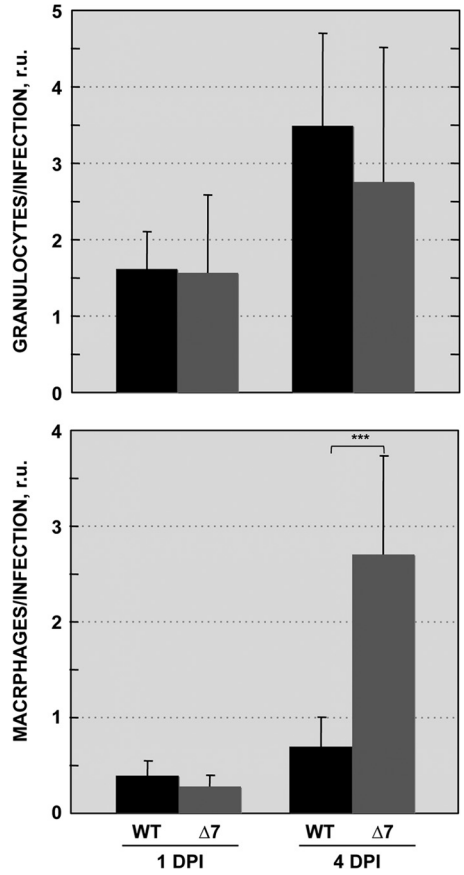

FIG 9 Quantification of the leukocyte/infection ratio in lung sections from infected animals. The leukocyte signal (immunofluorescence red channel) was estimated in lung sections from infected animals. The positive area for granulocytes (upper panel) or macrophages (lower panel) signal relative to the positive area for TGEV infection (immunofluorescence green channel) signal was calculated using MetaMorph software. Error bars indicate the standard deviations from 20 observed fields in 10 independent samples. ***, $P < 0.001$. r.u., relative units.

previous study (47), which only displays respiratory tropism causing lung damage and no apparent gut infection. TGEV is a porcine virus, and the work presented here has been performed using the natural host, which is immunologically more similar to humans (>80%) than mice (<10%) (69). Therefore, our findings might be informative for the conserved pathways leading to increased pathology both in pigs and humans.

TGEV protein 7 reduced the dsRNA triggered antiviral response (47). As a consequence, rTGEV-Δ7 infection caused enhanced cell death, cellular RNA degradation, and protein synthesis shutoff (47). The results presented here were most likely not conditioned by these effects, since both microarray and RT-qPCR analyses were performed using the same amount of total intracellular RNA of equal quality, extracted from living cells attached to the plate. In addition, microarray data normalization corrects any differences in mRNA amount between samples, and in RT-qPCR the mRNA levels always referred to the amount of GUSB that correlated with the percentage of living cells. In the case of cytokine measurements in the supernatants of infected cells, cell death most likely did not significantly affect quantifications, since similar differences between rTGEV-wt and rTGEV-Δ7 viruses were obtained when intracellular protein extracts were used for ELISAs (data not shown). In addition, up to a 20-fold increase in mRNA accumulation led to an increase no more than 3.5-fold in protein levels when rTGEV-wt and rTGEV-Δ7 infections were compared (Fig. 4). Similarly, differences up to 10^3-fold in mRNA levels led to no more than 10-fold differences in protein accumulation, when comparing mock-infected cells to rTGEV-wt-infected cells (Fig. 4). This result suggested that shutoff caused by the rTGEV-Δ7 virus was not affecting cytokine measurements.

The infection of swine by rTGEV-Δ7 virus caused higher lung damage than that caused by rTGEV-wt (47). Neutrophils and macrophages have been proposed to cause lung damage during most cases of acute lung injury and ARDS (70). Granulocytes were recruited to the TGEV-infected lungs, both in the presence and in absence of protein 7, suggesting that they play a role in TGEV-induced inflammation. *In vivo*, rTGEV-Δ7 infection caused an increased expression of proinflammatory cytokines such as TNF, CCL2, and CCL5, whose main function is macrophage recruitment and activation (26, 71, 72). In addition, at least *in vitro*, rTGEV-Δ7 infection induced the expression of CD40 receptor (Fig. 2B), which has been involved in macrophage activation (73). In agreement with these results, in the lungs from rTGEV-Δ7-infected animals, an increase in macrophage recruitment and activation was observed compared to the rTGEV-wt-infected animals. In line with these data, MHV infection of CCL5 receptor knockout mice causes a reduced pathology due to a decrease in macrophage recruitment (74). In addition, it was recently reported that coronavirus infection of transgenic mice expressing CCL2 led to an enhanced pathology leading to death, caused by a dysregulated immune response without effective virus clearance (75). Similar observations were obtained after influenza virus infection of CCL2 ($CCR2^{-/-}$) or CCL5 ($CCR5^{-/-}$) receptors knockout mice (76). Lung pathology was reduced in influenza virus-infected $CCR2^{-/-}$ mice, since monocyte recruitment is severely impaired in these animals (76). In contrast, $CCR5^{-/-}$ infected mice showed increased mortality associated with elevated macrophage infiltration in the lungs due to an increased expression of CCL2 (76). The data obtained in the present work suggested that macrophages were involved in the enhanced inflammation produced during infection in the absence of protein 7 and were in agreement with the role of CCL2 in the immunopathology mediated by macrophage recruitment.

An exacerbated proinflammatory cytokine production and an excessive immune cell recruitment leading to tissue destruction contributing to virus caused pathology, similar to that observed after rTGEV-Δ7 infection, has been described for several viral infections (77–79). This immunopathology, known as "cytokine storm," could be the cause for the extreme virulence of several viruses, such as pandemic influenza virus H5N1 or SARS-CoV (80). Once started, increased proinflammatory cytokines could continue driving immunopathology progression, even in the absence of viral replication. In fact, lung damage in SARS-CoV-infected patients persists after virus titer reduction, suggesting that pathology is mainly caused by the immune response (81). Similarly, in RSV infections, the severity of the infection has been correlated with CCL2 and CCL5 expression (72). In addition, cellular recruitment, mediated by cytokine expression, has been considered responsible for damaging both infected and uninfected areas of the lung (26). In line with these observations, rTGEV-Δ7

infection caused a "cytokine storm" that led to a progression in lung damage (47).

In the absence of protein 7, an increased expression in IFN-β, IFN-stimulated genes (ISGs), and proinflammatory genes was observed. Similar upregulation of genes was reported for viruses with mutations in virus-encoded IFN antagonists, such as influenza virus with the mutated NS1 gene (82, 83). To date, virus-encoded IFN antagonists were mainly analyzed in overexpression studies, and the activity of only around half of these antagonists was demonstrated in the context of viral infection (27). The IFN antagonist activity of TGEV protein 7 decreasing IFN-β production was demonstrated here, in the context of viral infection, although more studies are required to further determine the characteristics and mechanism of IFN antagonism by protein 7.

As expected for a virus defective in an IFN antagonism pathway, the rTGEV-Δ7 mutant virus was more sensitive to IFN-β-induced antiviral effects (data not shown). Nevertheless, the rTGEV-Δ7 virus underwent efficient replication despite increased IFN-β production. This was explained by the amount of IFN-β produced by ST cells, being 10^3-fold lower than the minimal concentration required for decreasing TGEV replication (data not shown). Most likely, this result was a consequence of the presence of other virus-encoded IFN antagonists in both rTGEV-wt and rTGEV-Δ7 genomes.

We have previously shown that TGEV protein 7 limited RNase L activation and eIF2α phosphorylation through its binding to PP1 phosphatase (47). RNase L has been involved in the IFN response, since cells deficient in this enzyme, infected with different viruses, produce lower IFN-β amounts than normal cells (23). It was proposed that the RNA degradation products generated by RNase L are recognized by RIG-I, acting as amplifiers of IFN production (23). In fact, the direct implication of RNase L on IFN production has been recently demonstrated using an MHV accessory protein ns2 mutant virus (24). In addition, PKR has also been recently involved in the amplification of innate immune response through a translational control mechanism, dependent on eIF2α phosphorylation, leading to increased IFN-β production and NF-κB activation (84). Therefore, the increased IFN-β and proinflammatory cytokines production observed during rTGEV-Δ7 infection, in the absence of protein 7, could be explained in the context of the previously proposed TGEV protein 7 mechanism of action, highlighting the role of RNase L and eIF2α phosphorylation in innate immunity. The results presented here confirm the role of CoV accessory genes in the modulation of innate immune responses during infection. The tight regulation of deleterious inflammatory responses by virus-encoded proteins seems to modulate both virus and host survival.

ACKNOWLEDGMENTS

We thank J. Dominguez for providing antibodies for macrophages and H. T. Reyburn for critical reading of the manuscript. We also thank M. González, C. M. Sánchez, R. Fernández, and S. Ros for technical assistance.

This study was supported by grants from the Ministry of Science and Innovation of Spain (BIO2010-16705), the U.S. National Institutes of Health (PO1 A1060699), and the European Community's Seventh Framework Programme (FP7/2007-2013) under the projects EMPERIE (EC grant agreement number 223498) and PoRRSCon (EC grant agreement number 245141). M.B. was supported by a contract from Consejo Superior de Investigaciones Cientificas. S.Z. and J.L.G.C. received contracts from the EU.

REFERENCES

1. **Enjuanes L, Gorbalenya AE, de Groot RJ, Cowley JA, Ziebuhr J, Snijder EJ.** 2008. The *Nidovirales*, p 419–430. *In* Mahy BWJ, Van Regenmortel M, Walker P, Majumder-Russell D (ed), Encyclopedia of virology, 3rd ed. Elsevier, Ltd, Oxford, England.
2. **Masters PS.** 2006. The molecular biology of coronaviruses. Adv. Virus Res. **66:**193–292.
3. **de Groot RJ, Baker SC, Baric R, Enjuanes L, Gorbalenya AE, Holmes KV, Perlman S, Poon L, Rottier PJM, Talbot PJ, Woo PCY, Ziebuhr J.** 2012. *Coronaviridae*, p 774–796. *In* King AMQ, Adams MJ, Carstens EB, Lefkowitz EJ (ed), Virus taxonomy: ninth report of the International Committee on Taxonomy of Viruses. Elsevier Academic Press, Inc, San Diego, CA.
4. **Woo PC, Lau SK, Lam CS, Lau CC, Tsang AK, Lau JH, Bai R, Teng JL, Tsang CC, Wang M, Zheng BJ, Chan KH, Yuen KY.** 2012. Discovery of seven novel mammalian and avian coronaviruses in the genus *Deltacoronavirus* supports bat coronaviruses as the gene source of *Alphacoronavirus* and *Betacoronavirus* and avian coronaviruses as the gene source of *Gammacoronavirus* and *Deltacoronavirus*. J. Virol. **86:**3995–4008.
5. **Denison MR.** 1999. The common cold: rhinoviruses and coronaviruses, p 253–280. *In* Dolin R, Wright PF (ed), Viral infections of the respiratory tract, vol 127. Marcel Dekker, Inc, New York, NY.
6. **Drosten C, Gunther S, Preiser W, van der Werf S, Brodt HR, Becker S, Rabenau H, Panning M, Kolesnikova L, Fouchier RA, Berger A, Burguiere AM, Cinatl J, Eickmann M, Escriou N, Grywna K, Kramme S, Manuguerra JC, Muller S, Rickerts V, Sturmer M, Vieth S, Klenk HD, Osterhaus AD, Schmitz H, Doerr HW.** 2003. Identification of a novel coronavirus in patients with severe acute respiratory syndrome. N. Engl. J. Med. **348:**1967–1976.
7. **Holmes KV, Enjuanes L.** 2003. The SARS coronavirus: a postgenomic era. Science **300:**1377–1378.
8. **Bermingham A, Chand M, Brown C, Aarons E, Tong C, Langrish C, Hoschler K, Brown K, Galiano M, Myers R, Pebody R, Green H, Boddington N, Gopal R, Price N, Newsholme W, Drosten C, Fouchier R, Zambon M.** 2012. Severe respiratory illness caused by a novel coronavirus, in a patient transferred to the United Kingdom from the Middle East, September 2012. Euro Surveill. **17:**20290.
9. **Zaki AM, van Boheemen S, Bestebroer TM, Osterhaus AD, Fouchier RA.** 2012. Isolation of a novel coronavirus from a man with pneumonia in Saudi Arabia. N. Engl. J. Med. doi:10.1056/NEJMoa1211721.
10. **Perlman S, Pewe L.** 1998. Role of CTL escape mutants in demyelination induced by mouse hepatitis virus, strain JHM. Adv. Exp. Med. Biol. **440:** 515–520.
11. **Brierley I, Digard P, Inglis SC.** 1989. Characterization of an efficient coronavirus ribosomal frameshifting signal: requirement for an RNA pseudoknot. Cell **57:**537–547.
12. **Perlman S, Netland J.** 2009. Coronaviruses post-SARS: update on replication and pathogenesis. Nat. Rev. Microbiol. **7:**439–450.
13. **Yount B, Roberts RS, Sims AC, Deming D, Frieman MB, Sparks J, Denison MR, Davis N, Baric RS.** 2005. Severe acute respiratory syndrome coronavirus group-specific open reading frames encode nonessential functions for replication in cell cultures and mice. J. Virol. **79:**14909–14922.
14. **DeDiego ML, Pewe L, Alvarez E, Rejas MT, Perlman S, Enjuanes L.** 2008. Pathogenicity of severe acute respiratory coronavirus deletion mutants in hACE-2 transgenic mice. Virology **376:**379–389.
15. **DeDiego ML, Nieto-Torres JL, Jimenez-Guardeno JM, Regla-Nava JA, Alvarez E, Oliveros JC, Zhao J, Fett C, Perlman S, Enjuanes L.** 2011. Severe acute respiratory syndrome coronavirus envelope protein regulates cell stress response and apoptosis. PLoS Pathog. **7:**e1002315. doi:10.1371/journal.ppat.1002315.
16. **DeDiego ML, Alvarez E, Almazan F, Rejas MT, Lamirande E, Roberts A, Shieh WJ, Zaki SR, Subbarao K, Enjuanes L.** 2007. A severe acute respiratory syndrome coronavirus that lacks the E gene is attenuated in vitro and in vivo. J. Virol. **81:**1701–1713.
17. **Tangudu C, Olivares H, Netland J, Perlman S, Gallagher T.** 2007. Severe acute respiratory syndrome coronavirus protein 6 accelerates murine coronavirus infections. J. Virol. **81:**1220–1229.
18. **Pewe L, Zhou H, Netland J, Tangudu C, Olivares H, Shi L, Look D, Gallagher T, Perlman S.** 2005. A severe acute respiratory syndrome-associated coronavirus-specific protein enhances virulence of an attenuated murine coronavirus. J. Virol. **79:**11335–11342.

19. **Medzhitov R, Janeway CA, Jr.** 1997. Innate immunity: the virtues of a nonclonal system of recognition. Cell **91:**295–298.
20. **Gantier MP, Williams BR.** 2007. The response of mammalian cells to double-stranded RNA. Cytokine Growth Factor Rev. **18:**363–371.
21. **Ishii KJ, Koyama S, Nakagawa A, Coban C, Akira S.** 2008. Host innate immune receptors and beyond: making sense of microbial infections. Cell Host Microbe **3:**352–363.
22. **Jensen S, Thomsen AR.** 2012. Sensing of RNA viruses: a review of innate immune receptors involved in recognizing RNA virus invasion. J. Virol. **86:**2900–2910.
23. **Malathi K, Dong B, Gale M, Jr, Silverman RH.** 2007. Small self-RNA generated by RNase L amplifies antiviral innate immunity. Nature **448:** 816–819.
24. **Zhao L, Jha BK, Wu A, Elliott R, Ziebuhr J, Gorbalenya AE, Silverman RH, Weiss SR.** 2012. Antagonism of the interferon-induced OAS-RNase L pathway by murine coronavirus ns2 protein is required for virus replication and liver pathology. Cell Host Microbe **11:**607–616.
25. **Bonjardim CA, Ferreira PC, Kroon EG.** 2009. Interferons: signaling, antiviral and viral evasion. Immunol. Lett. **122:**1–11.
26. **Vareille M, Kieninger E, Edwards MR, Regamey N.** 2011. The airway epithelium: soldier in the fight against respiratory viruses. Clin. Microbiol. Rev. **24:**210–229.
27. **Versteeg GA, Garcia-Sastre A.** 2010. Viral tricks to grid-lock the type I interferon system. Curr. Opin. Microbiol. **13:**508–516.
28. **Kopecky-Bromberg SA, Martinez-Sobrido L, Frieman M, Baric RA, Palese P.** 2007. Severe acute respiratory syndrome coronavirus open reading frame (ORF) 3b, ORF 6, and nucleocapsid proteins function as interferon antagonists. J. Virol. **81:**548–557.
29. **Lu X, Pan J, Tao J, Guo D.** 2011. SARS-CoV nucleocapsid protein antagonizes IFN-beta response by targeting initial step of IFN-beta induction pathway, and its C-terminal region is critical for the antagonism. Virus Genes **42:**37–45.
30. **Ye Y, Hauns K, Langland JO, Jacobs BL, Hogue BG.** 2007. Mouse hepatitis coronavirus A59 nucleocapsid protein is a type I interferon antagonist. J. Virol. **81:**2554–2563.
31. **Siu KL, Kok KH, Ng MH, Poon VK, Yuen KY, Zheng BJ, Jin DY.** 2009. Severe acute respiratory syndrome coronavirus M protein inhibits type I interferon production by impeding the formation of TRAF3.TANK.TBK1/IKKεcomplex. J. Biol. Chem. **284:**16202–16209.
32. **Narayanan K, Huang C, Lokugamage K, Kamitani W, Ikegami T, Tseng CT, Makino S.** 2008. Severe acute respiratory syndrome coronavirus nsp1 suppresses host gene expression, including that of type I interferon, in infected cells. J. Virol. **82:**4471–4479.
33. **Kamitani W, Huang C, Narayanan K, Lokugamage KG, Makino S.** 2009. A two-pronged strategy to suppress host protein synthesis by SARS coronavirus Nsp1 protein. Nat. Struct. Mol. Biol. **16:**1134–1140.
34. **Wathelet MG, Orr M, Frieman MB, Baric RS.** 2007. Severe acute respiratory syndrome coronavirus evades antiviral signaling: role of nsp1 and rational design of an attenuated strain. J. Virol. **81:**11620–11633.
35. **Zust R, Cervantes-Barragan L, Kuri T, Blakqori G, Weber F, Ludewig B, Thiel V.** 2007. Coronavirus nonstructural protein 1 is a major pathogenicity factor: implications for the rational design of coronavirus vaccines. PLoS Pathog. **3:**e109. doi:10.1371/journal.ppat.0030109.
36. **Eriksson KK, Cervantes-Barragan L, Ludewig B, Thiel V.** 2008. Mouse hepatitis virus liver pathology is dependent on ADP-ribose-1-phosphatase, a viral function conserved in the alpha-like supergroup. J. Virol. **82:**12325–12334.
37. **Frieman M, Ratia K, Johnston RE, Mesecar AD, Baric RS.** 2009. Severe acute respiratory syndrome coronavirus papain-like protease ubiquitin-like domain and catalytic domain regulate antagonism of IRF3 and NF-κB signaling. J. Virol. **83:**6689–6705.
38. **Kuri T, Eriksson KK, Putics A, Zust R, Snijder EJ, Davidson AD, Siddell SG, Thiel V, Ziebuhr J, Weber F.** 2011. The ADP-ribose-1′′-monophosphatase domains of severe acute respiratory syndrome coronavirus and human coronavirus 229E mediate resistance to antiviral interferon responses. J. Gen. Virol. **92:**1899–1905.
39. **Wang G, Chen G, Zheng D, Cheng G, Tang H.** 2011. PLP2 of mouse hepatitis virus A59 (MHV-A59) targets TBK1 to negatively regulate cellular type I interferon signaling pathway. PLoS One **6:**e17192. doi:10.1371/journal.pone.0017192.
40. **Zust R, Cervantes-Barragan L, Habjan M, Maier R, Neuman BW, Ziebuhr J, Szretter KJ, Baker SC, Barchet W, Diamond MS, Siddell SG, Ludewig B, Thiel V.** 2011. Ribose 2′-*O*-methylation provides a molecular signature for the distinction of self and non-self mRNA dependent on the RNA sensor Mda5. Nat. Immunol. **12:**137–143.
41. **Koetzner CA, Kuo L, Goebel SJ, Dean AB, Parker MM, Masters PS.** 2010. Accessory protein 5a is a major antagonist of the antiviral action of interferon against murine coronavirus. J. Virol. **84:**8262–8274.
42. **Zhao L, Rose KM, Elliott R, Van Rooijen N, Weiss SR.** 2011. Cell type-specific type I interferon antagonism influences organ tropism of murine coronavirus. J. Virol. **85:**10058–10068.
43. **Frieman M, Yount B, Heise M, Kopecky-Bromberg SA, Palese P, Baric RS.** 2007. Severe acute respiratory syndrome coronavirus ORF6 antagonizes STAT1 function by sequestering nuclear import factors on the rough endoplasmic reticulum/Golgi membrane. J. Virol. **81:**9812–9824.
44. **Brian DA, Baric RS.** 2005. Coronavirus genome structure and replication. Curr. Top. Microbiol. Immunol. **287:**1–30.
45. **Enjuanes L, Almazan F, Ortego J.** 2003. Virus-based vectors for gene expression in mammalian cells: coronavirus, p 151–168. *In* Makrides SC (ed), Gene transfer and expression in mammalian cells. Elsevier Science B.V., Amsterdam, Netherlands.
46. **Sola I, Alonso S, Zuniga S, Balasch M, Plana-Duran J, Enjuanes L.** 2003. Engineering the transmissible gastroenteritis virus genome as an expression vector inducing lactogenic immunity. J. Virol. **77:**4357–4369.
47. **Cruz JLG, Sola I, Becares M, Alberca B, Plana J, Enjuanes L, Zuniga S.** 2011. Coronavirus gene 7 counteracts host defenses and modulates virus virulence. PLoS Pathog. **7:**e1002090. doi:10.1371/journal.ppat.1002090.
48. **McClurkin AW, Norman JO.** 1966. Studies on transmissible gastroenteritis of swine. II. Selected characteristics of a cytopathogenic virus common to five isolates from transmissible gastroenteritis. Can. J. Comp. Med. Vet. Sci. **30:**190–198.
49. **Irizarry RA, Bolstad BM, Collin F, Cope LM, Hobbs B, Speed TP.** 2003. Summaries of Affymetrix GeneChip probe level data. Nucleic Acids Res. **31:**e15.
50. **Smyth GK.** 2004. Linear models and empirical bayes methods for assessing differential expression in microarray experiments. Stat. Appl. Genet. Mol. Biol. **3:**Article3.
51. **Benjamini Y, Hochberg Y.** 1995. Controlling the false discovery rate: a practical and powerful approach to multiple testing. J. Roy. Stat. Soc. B **57:**289–300.
52. **Tsai S, Cassady JP, Freking BA, Nonneman DJ, Rohrer GA, Piedrahita JA.** 2006. Annotation of the Affymetrix porcine genome microarray. Anim. Genet. **37:**423–424.
53. **da Huang W, Sherman BT, Lempicki RA.** 2009. Systematic and integrative analysis of large gene lists using DAVID bioinformatics resources. Nat. Protoc. **4:**44–57.
54. **da Huang W, Sherman BT, Lempicki RA.** 2009. Bioinformatics enrichment tools: paths toward the comprehensive functional analysis of large gene lists. Nucleic Acids Res. **37:**1–13.
55. **Ashburner M, Ball CA, Blake JA, Botstein D, Butler H, Cherry JM, Davis AP, Dolinski K, Dwight SS, Eppig JT, Harris MA, Hill DP, Issel-Tarver L, Kasarskis A, Lewis S, Matese JC, Richardson JE, Ringwald M, Rubin GM, Sherlock G.** 2000. Gene ontology: tool for the unification of biology. Gene Ontology Consortium. Nat. Genet. **25:**25–29.
56. **Zuñiga S, Cruz JL, Sola I, Mateos-Gomez PA, Palacio L, Enjuanes L.** 2010. Coronavirus nucleocapsid protein facilitates template switching and is required for efficient transcription. J. Virol. **84:**2169–2175.
57. **Bustin SA, Benes V, Garson JA, Hellemans J, Huggett J, Kubista M, Mueller R, Nolan T, Pfaffl MW, Shipley GL, Vandesompele J, Wittwer CT.** 2009. The MIQE guidelines: minimum information for publication of quantitative real-time PCR experiments. Clin. Chem. **55:**611–622.
58. **Sanchez CM, Izeta A, Sanchez-Morgado JM, Alonso S, Sola I, Balasch M, Plana-Duran J, Enjuanes L.** 1999. Targeted recombination demonstrates that the spike gene of transmissible gastroenteritis coronavirus is a determinant of its enteric tropism and virulence. J. Virol. **73:**7607–7618.
59. **Domenech N, Rodriguez-Carreno MP, Filgueira P, Alvarez B, Chamorro S, Dominguez J.** 2003. Identification of porcine macrophages with monoclonal antibodies in formalin-fixed, paraffin-embedded tissues. Vet. Immunol. Immunopathol. **94:**77–81.
60. **Chianini F, Majo N, Segales J, Dominguez J, Domingo M.** 2001. Immunohistological study of the immune system cells in paraffin-embedded tissues of conventional pigs. Vet. Immunol. Immunopathol. **82:**245–255.
61. **Laude H, Charley B, Gelfi J.** 1984. Replication of transmissible gastroenteritis coronavirus (TGEV) in swine alveolar macrophages. J. Gen. Virol. **65:**327–335.

62. **Guzylack-Piriou L, Piersma S, McCullough K, Summerfield A.** 2006. Role of natural interferon-producing cells and T lymphocytes in porcine monocyte-derived dendritic cell maturation. Immunology **118:**78–87.
63. **Riffault S, Carrat C, van Reeth K, Pensaert M, Charley B.** 2001. Interferon-alpha-producing cells are localized in gut-associated lymphoid tissues in transmissible gastroenteritis virus (TGEV)-infected piglets. Vet. Res. **32:**71–79.
64. **Calzada-Nova G, Schnitzlein W, Husmann R, Zuckermann FA.** 2010. Characterization of the cytokine and maturation responses of pure populations of porcine plasmacytoid dendritic cells to porcine viruses and Toll-like receptor agonists. Vet. Immunol. Immunopathol. **135:**20–33.
65. **Rouse BT, Sehrawat S.** 2010. Immunity and immunopathology to viruses: what decides the outcome? Nat. Rev. Immunol. **10:**514–526.
66. **Zampieri CA, Sullivan NJ, Nabel GJ.** 2007. Immunopathology of highly virulent pathogens: insights from Ebola virus. Nat. Immunol. **8:**1159–1164.
67. **Huynh KK, Eskelinen EL, Scott CC, Malevanets A, Saftig P, Grinstein S.** 2007. LAMP proteins are required for fusion of lysosomes with phagosomes. EMBO J. **26:**313–324.
68. **Saif LJ.** 1996. Mucosal immunity: an overview and studies of enteric and respiratory coronavirus infections in a swine model of enteric disease. Vet. Immunol. Immunopathol. **54:**163–169.
69. **Meurens F, Summerfield A, Nauwynck H, Saif L, Gerdts V.** 2012. The pig: a model for human infectious diseases. Trends Microbiol. **20:**50–57.
70. **Matthay MA, Zemans RL.** 2011. The acute respiratory distress syndrome: pathogenesis and treatment. Annu. Rev. Pathol. **6:**147–163.
71. **Deshmane SL, Kremlev S, Amini S, Sawaya BE.** 2009. Monocyte chemoattractant protein-1 (MCP-1): an overview. J. Interferon Cytokine Res. **29:**313–326.
72. **Amanatidou V, Zaravinos A, Apostolakis S, Spandidos DA.** 2011. Chemokines in respiratory viral infections: focus on their diagnostic and therapeutic potential. Crit. Rev. Immunol. **31:**341–356.
73. **Hashimoto N, Kawabe T, Imaizumi K, Hara T, Okamoto M, Kojima K, Shimokata K, Hasegawa Y.** 2004. CD40 plays a crucial role in lipopolysaccharide-induced acute lung injury. Am. J. Respir. Cell Mol. Biol. **30:**808–815.
74. **Glass WG, Liu MT, Kuziel WA, Lane TE.** 2001. Reduced macrophage infiltration and demyelination in mice lacking the chemokine receptor CCR5 following infection with a neurotropic coronavirus. Virology **288:**8–17.
75. **Trujillo JA, Fleming EL, Perlman S.** 2013. Transgenic CCL2 expression in the central nervous system results in a dysregulated immune response and enhanced lethality after coronavirus infection. J. Virol. **87:**2376–2389.
76. **Dawson TC, Beck MA, Kuziel WA, Henderson F, Maeda N.** 2000. Contrasting effects of CCR5 and CCR2 deficiency in the pulmonary inflammatory response to influenza A virus. Am. J. Pathol. **156:**1951–1959.
77. **Huang KJ, Su IJ, Theron M, Wu YC, Lai SK, Liu CC, Lei HY.** 2005. An interferon-gamma-related cytokine storm in SARS patients. J. Med. Virol. **75:**185–194.
78. **Theron M, Huang KJ, Chen YW, Liu CC, Lei HY.** 2005. A probable role for IFN-gamma in the development of a lung immunopathology in SARS. Cytokine **32:**30–38.
79. **Walsh KB, Teijaro JR, Wilker PR, Jatzek A, Fremgen DM, Das SC, Watanabe T, Hatta M, Shinya K, Suresh M, Kawaoka Y, Rosen H, Oldstone MB.** 2011. Suppression of cytokine storm with a sphingosine analog provides protection against pathogenic influenza virus. Proc. Natl. Acad. Sci. U. S. A. **108:**12018–12023.
80. **Tisoncik JR, Korth MJ, Simmons CP, Farrar J, Martin TR, Katze MG.** 2012. Into the eye of the cytokine storm. Microbiol. Mol. Biol. Rev. **76:**16–32.
81. **Peiris JS, Chu CM, Cheng VC, Chan KS, Hung IF, Poon LL, Law KI, Tang BS, Hon TY, Chan CS, Chan KH, Ng JS, Zheng BJ, Ng WL, Lai RW, Guan Y, Yuen KY.** 2003. Clinical progression and viral load in a community outbreak of coronavirus-associated SARS pneumonia: a prospective study. Lancet **361:**1767–1772.
82. **Fernandez-Sesma A, Marukian S, Ebersole BJ, Kaminski D, Park MS, Yuen T, Sealfon SC, Garcia-Sastre A, Moran TM.** 2006. Influenza virus evades innate and adaptive immunity via the NS1 protein. J. Virol. **80:**6295–6304.
83. **Haye K, Burmakina S, Moran T, Garcia-Sastre A, Fernandez-Sesma A.** 2009. The NS1 protein of a human influenza virus inhibits type I interferon production and the induction of antiviral responses in primary human dendritic and respiratory epithelial cells. J. Virol. **83:**6849–6862.
84. **McAllister CS, Taghavi N, Samuel CE.** 2012. Protein kinase PKR amplification of interferon beta induction occurs through initiation factor eIF-2α-mediated translational control. J. Biol. Chem. **287:**36384–36392.